Plasma Sources Science and Technology

PAPER

Impact of surface charges on energy deposition in surface dielectric barrier discharge: a modeling investigation

To cite this article: Chenhua Ren *et al* 2023 *Plasma Sources Sci. Technol.* **32** 025004

IOP Publishing

Plasma Sources Science and Technology

Plasma Sources Sci. Technol. **32** (2023) 025004 (13pp)

https://doi.org/10.1088/1361-6595/acb4b9

Impact of surface charges on energy deposition in surface dielectric barrier discharge: a modeling investigation

Chenhua Ren[1,2], Bangdou Huang[2,*], Cheng Zhang[2,3,*], Bo Qi[1], Weijiang Chen[4] and Tao Shao[2,3]

[1] North China Electric Power University, Beijing 102206, People's Republic of China

[2] Beijing International S&T Cooperation Base for Plasma Science and Energy Conversion, Institute of Electrical Engineering, Chinese Academy of Sciences, Beijing 100190, People's Republic of China

[3] University of Chinese Academy of Sciences, Beijing 100049, People's Republic of China

[4] State Grid Corporation of China, Beijing 100031, People's Republic of China

E-mail: huangbangdou@mail.iee.ac.cn and zhangcheng@mail.iee.ac.cn

Received 7 October 2022, revised 22 December 2022

Accepted for publication 19 January 2023

Published 14 February 2023

Abstract

Surface charges have significant impact on the evolution of surface dielectric barrier discharge (SDBD). In this work, the role of residual surface charges on repetitively nanosecond pulsed SDBD in atmospheric air is investigated using a two-dimensional fluid model, based on the assumption of preserving the distribution of surface charges at the end of the previous high voltage (HV) pulse. In the bipolar mode when the polarity of residual surface charges is opposite to that of the current HV pulse, a lower breakdown voltage and more deposited energy can be observed, showing an obvious enhancement of SDBD. In the unipolar mode, residual surface charges suppress the development of discharges and energy deposition. It is found that more residual surface charges are accumulated during the negative pulsed discharge, which have a more pronounced effect on the subsequent positive pulsed one. This is explained by the fact that the negative surface streamers directly contact the dielectric and charge it, while the positive surface streamers float above the dielectric, forming a ion-rich region near the surface. The results in this work demonstrate the mechanism of how residual surface charges affect discharge dynamics, which can be utilized to regulate energy deposition in SDBDs.

Keywords: nanosecond pulsed discharge, surface dielectric barrier discharge, residual surface charge, plasma modeling

(Some figures may appear in colour only in the online journal)

1. Introduction

Surface dielectric barrier discharge (SDBD) at atmospheric pressure has been intensively studied due to its potential use in various fields, such as plasma-assisted ignition and combustion [1, 2], surface treatment [3, 4], and flow control [5, 6]. Additionally, surface discharge occurs easily at the triple point (gas/metal/dielectric interface) [7], which greatly threatens the safe operation of the high-voltage (HV) transmission systems [8, 9]. Further investigation of the breakdown process of SDBD is important for its potential applications.

Driven by sinusoidal alternating-current (AC) or repetitively nanosecond pulsed HV, streamers start from the HV electrode and propagate along the dielectric [10, 11], with a strong coupling between the gas and surface [12]. Plasma–dielectric interaction is related to deposition of surface charges [13, 14], which distorts the electric field distribution and has a big impact on discharge evolution [15–17]. Due to the long decay time of the surface charges (even up to several hours

* Authors to whom any correspondence should be addressed.

depending on the conductivity of dielectric used) [18, 19], its accumulation effect is crucial for subsequent discharges, especially under pulsed excitation [20–22].

Recently, electric field-induced second harmonic (E-FISH), as a non-intrusive diagnostic method with a spatial resolution down to micrometers and a temporal resolution down to subnanoseconds, has been implemented for electric field measurement in SDBDs [23]. It is impressive to observe that the accumulation of surface charges during the previous pulses is a significant factor affecting the electric field in the subsequent discharges, even with relatively low pulse repetition rates [12, 23]. The contribution of surface charges has also been observed in atmospheric pressure plasma jets with the existence of dielectrics [24]. In addition, the Pockels-effect method has also been realized to trace the surface charges [25–27].

Different numerical models have been developed, such as the particle-in-cell (PIC)/Monte Carlo collision model [14, 28, 29], fluid model [30–34], and hybrid model with a kinetic treatment of energetic electrons [35, 36] to study the plasma–dielectric interaction and reveal the streamer dynamics along dielectric surface for both polarities. It is demonstrated that the deposition of surface charges generates electric field components parallel to the dielectric surface and supports the propagation of surface discharges, which play a significant role in the case of the single-pulse discharge [34, 37].

Nevertheless, in the reality of both low-frequency AC and repetitively pulsed SDBD, there is the existence of residual surface charges with complex distribution and evolution dynamics, which will significantly influence the following breakdown [17, 36, 38–40]. A series of self-consistent models coupling discharge and fluid flow have been established to study the AC SDBD [16, 41, 42], showing the strong impact of residual surface charges on the discharge evolution between the positive and negative phases [16, 17].

Even so, the impact of surface charge accumulation on the discharge development and energy deposition in pulsed SDBD is still not fully understood. Since numerical simulation of repetitively pulsed SDBD on a full scale is extremely time consuming and has not yet been done, a reasonable description of the impact of residual surface charges at a relatively low computational cost may benefit further understanding of the intrinsic properties of SDBD.

As the impacts of surface charges have been well demonstrated in experimental investigations but convictive modeling investigation on this effect is still lacking, the aim of this work is to study the dynamic behavior of surface charges during nanosecond HV pulses and their impact on subsequent discharge by numerical modeling. To introduce the residual charges in repetitively pulsed discharges, we preserve the distribution of surface charges at the end of the previous HV pulse. Based on this assumption, the breakdown evolutions and energy deposition are presented and analyzed for both polarities, with and without the residual surface charges.

2. Model description

2.1. Governing equations

The fluid modeling of SDBDs is based on the 2D PASSKEy (PArallel Streamer Solver with KinEtics) code [43]. Detailed numerical methods and benchmarks can be found in [11, 44]. In this section, we briefly show the equations and treatments of the code to consider the impact of residual surface charges on the subsequent discharge.

Continuity equations with drift-diffusion approximate for species are solved as follows:

$$\frac{\partial n_i}{\partial t} + \nabla \cdot \mathbf{\Gamma}_i = S_i + S_{ph},\ i = 1, 2, \ldots, N_{total} \tag{1}$$

$$\mathbf{\Gamma}_i = -D_i \nabla n_i - \left(\frac{q_i}{|q_i|}\right) \mu_i n_i \nabla \phi,\ i = 1, 2, \ldots, N_{charge} \tag{2}$$

$$\frac{\partial (n_e \in_m)}{\partial t} + \nabla \cdot \mathbf{\Gamma}_\in = -|q_e| \cdot E \cdot \mathbf{\Gamma}_e - P(\in_m) \tag{3}$$

$$\mathbf{\Gamma}_\in = -D_\in \nabla (n_e \in_m) - n_e \in_m \mu_\in E\ . \tag{4}$$

Here, n_i, q_i, $\mathbf{\Gamma}_i$, S_i, D_i, and μ_i are number density, charge, flux, source term due to gas-phase reactions, diffusion coefficient, and mobility of species i, respectively. S_{ph} is the photoionization source term. To obtain the fine structure of the plasma–dielectric interaction, the energy conservation equation is also coupled. n_e, q_e, ϵ_m, $\mathbf{\Gamma}_\epsilon$, D_ϵ, and μ_ϵ are the electron number density, elementary charge, mean electron energy, flux term, electron energy diffusion coefficient, and mobility, respectively. $\boldsymbol{E}$ is the electric field. Electron transport coefficients, reaction rates, and electron collision power lost $P(\epsilon_m)$ are calculated by Bolsig+ [45] based on the local mean energy approximation.

The photoionization source term S_{ph} for electrons and O+ 2 is calculated by three-term Helmholtz equations in air, with an assumption that ionization of oxygen molecules occurs by the radiation of nitrogen molecules in singlet states $b^1\Pi_u$, $b'^1\Sigma_u^+$, and $c_4'^1\Sigma_u^+$ [46]:

$$S_{\mathrm{ph}}(\vec{r}) = \sum_j S_{\mathrm{ph}}^j(\vec{r}) \tag{5}$$

$$\nabla^2 S_{\mathrm{ph}}^j(\vec{r}) - (\lambda_j p_{O_2})^2 S_{\mathrm{ph}}^j(\vec{r}) = -A_j p_{O_2}^2 I(\vec{r}) \tag{6}$$

where p_{O_2} is the partial pressure of O_2, $I(\vec{r})$ is the ionization source rate, and λ_j and A_j are the fitting parameters of photoionization functions and taken from [47], respectively.

The Poisson equation is solved with consideration of the dielectric surface charge density σ,

$$\nabla (\varepsilon_0 \varepsilon_r \nabla \phi) = -\rho - \sigma \tag{7}$$

$$\frac{\partial \sigma}{\partial t} = \sum_i q_i (-\nabla \cdot \mathbf{\Gamma}_i). \tag{8}$$

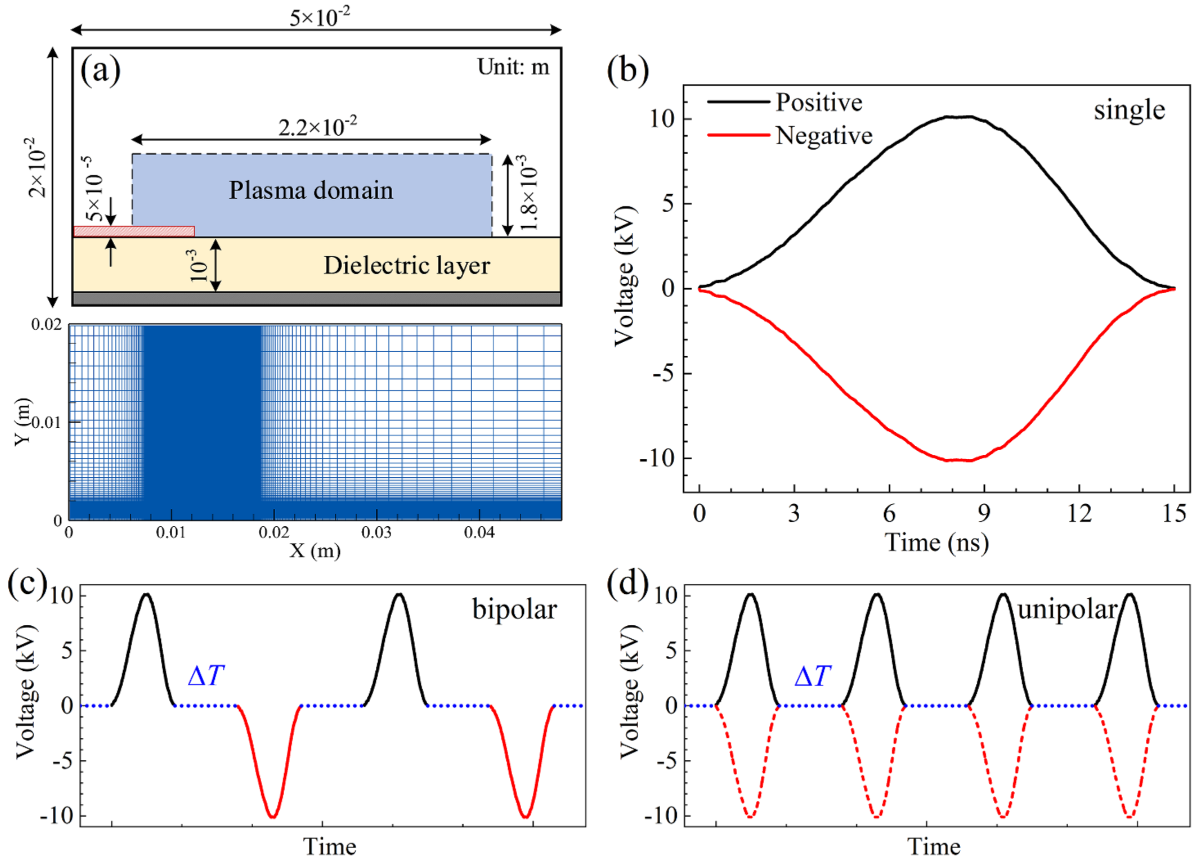

Figure 1. 2D computational domain and structured Cartesian mesh distribution (a). Input waveforms for fluid model in single (b), bipolar (c), and unipolar (d) modes.

2.2. Domain, waveforms, and assumptions

The 2D computational domain of 5 $\times$ 2 cm is shown in figure 1(a). The Poisson equation and Helmholtz equations are solved in the entire domain, while the continuity equations for species are only applied to the plasma domain to reduce the computational burden. The HV electrode (red region) with a thickness of 50 μm and the ground electrode (dark region) are separated by a dielectric layer ($\varepsilon_r = 4.2$) with a thickness of 1 mm. The discharge operates in atmospheric air with 300 K. The kinetics scheme for N_2/O_2 contains 15 species and 34 reactions, and has been successfully used in [11, 48]. Details can be found in [11]. Near the HV electrode and dielectric surface, 2–5 μm mesh size is adopted to resolve the thin surface streamers. The mesh size grows exponentially in the rest of the computational domain.

Figures 1(b)–(d) present waveforms of the positive and negative polarity pulses used in fluid modeling. These are similar to the waveform of a homemade bipolar nanosecond pulse generator, which has been used to generate SDBD in our previous work [49]. The pulse duration is approximately 300 ns and the peak voltage is 10 kV. As the input of the numerical model, the voltage waveform is scaled down 20 times in the time (narrower) to reduce the computational cost. Since the voltage waveform is an approximately Gaussian shape, a narrower pulse leads to both shorter rising and falling edge. The consequences include: (a) a shorter rising edge results in a higher mean electric field in the streamer head and consequently a larger propagation velocity [50, 51], and (b) a shorter falling edge leads to a faster potential drop on the HV electrode relative to the plasma channel, which may enhance the strength of the reverse electric field sustained near the HV electrode [16, 52, 53].

Although a single pulse (positive or negative polarity) is still applied in the fluid model, the impact of residual surface charges on subsequent discharge can be considered on the basis of the following assumptions. (a) Charge dissipation on the dielectric surface can last several seconds or even up to several hours [18, 19], which is much greater than the pulse interval ΔT (on the order of microseconds to milliseconds). Therefore, the decay of the surface charges can be neglected until the next pulse. The distribution of surface charges at the end of the previous pulse is set as the initial boundary condition for the next pulse along the dielectric surface. (b) The initial charge density in gas phase is taken as 10^{10} m^{-3} uniformly distributed in the plasma domain based on quasi-neutrality assumption.

2.3. Validation of assumptions

In order to validate these assumptions, the following analysis is performed. Three characteristic times should be considered, namely the relaxation time of surface charges τ_s, the recombination time between positive and negative ions (in gas phase)

τ_r, and the diffusion time of space charges to the dielectric surface τ_d, respectively.

τ_s is determined by the volume resistivity ρ_v [12]:

$$\tau_s = \varepsilon_0 \varepsilon_r \rho_v \quad (9)$$

For example, epoxy resin (relative dielectric constant $\varepsilon_r \approx 4.3$) has a volume resistivity τ_s on the order of 10^{10} Ω m and τ_s is approximately 0.4 s.

During the afterglow of atmospheric air, electrons are quickly transformed to O_2^- through the three-body attachment, with a rate coefficient of $k_{att} = 2 \times 10^{-41} \times (300/T_e)$ m^3 s^{-1} [54]. The characteristic time of electron decay $\tau_{att} = 1/(k_{att} \times [O_2] \times [O_2]) \approx 8.1 \times 10^{-8}$ s. Then, the recombination between positive (mainly O_4^+ [55]) and negative ions becomes dominant, $O_2^- + O_4^+ \rightarrow 3O_2$, $k_r = 10^{-13}$ m^3 s^{-1} [54]. With maximum charge density of around $10^{20} - 10^{21}$ m^{-3}, the ion recombination time $\tau_r = 1/(k_r \times [O_2^-])$ is around $10^{-8} - 10^{-7}$ s.

The competitive process of the ion recombination is diffusion to the dielectric surface. The total number density towards the dielectric surface $\Delta\sigma$ with given time τ_d can be estimated as

$$\Delta\sigma = -eD\frac{\partial n_i}{\partial y}\tau_d \quad (10)$$

Taking $D \approx 40/p$ cm^2 s^{-1} from [56], $p = 760$ Torr, $\partial n_i/\partial y \approx \Delta n_i/\Delta y$, $\Delta n_i \approx 10^{20}$ m^{-3}, and $\Delta y \approx 5 \times 10^{-5}$ m. As the surface charges deposited during the discharge period are on the order of $\sim 10^2$ nC cm^{-2}, it takes τ_d of $\sim 5.9 \times 10^{-6}$ s to achieve $\Delta\sigma/\sigma \sim 1\%$.

Based on this analysis, it can be seen that $\tau_s \gg \tau_d \gg \tau_r$. This means that the space charges are rapidly recombined after the discharge while a minor amount diffuses towards the surface, i.e. the neutralization of surface charges by ions in the gas phase can be ignored. Meanwhile, the surface charges deposited during the discharge period rarely decay between the pulse interval. Therefore, the assumptions in this work are valid.

In this work, we first calculate two discharge processes under the positive and negative pulses without pre-pulse, which are denoted as the single mode for both polarities. Then, these two cases are used as the pre-pulse for the subsequent discharge (positive or negative) to introduce the role of residual surface charges. For the current pulse, if the pre-pulse has an opposite polarity, it is denoted as the bipolar mode; otherwise, it is in the unipolar mode.

3. Results and discussion

3.1. Surface discharge dynamics

The typical distributions of the positive and negative SDBD at 6.5 ns (electron density and electric field) are shown in figure 2. The same value scales are used for both polarities.

For the positive polarity, the SDBD propagates against the direction of the electron drift [14, 36]. When the positive streamer approaches the dielectric surface, the loss term caused by electron drift to the discharge channel cannot be compensated by the source term of photoionization in bulk gas or ions/photons-induced secondary electron emission at the gas–solid interface [28, 33]. As a result, an ion-rich (or sheath-like) region with a thickness of 8–10 μm is left between the streamer front and the dielectric surface, where the electric field is very strong and above which the electric field intensity drops drastically.

For the negative polarity, the electron drift has the same direction with the SDBD propagation. The streamer contacts the dielectric and charges the surface negatively [36, 57], between which no gap is formed [14, 31, 36]. The distribution of negative space charges is quite diffuse and the electric field concentrates near the streamer front with a relative weak amplitude and near the HV electrode [36]. Since the electric field at the negative streamer front is much weaker than that of the positive one, the former develops much slower under similar operating conditions. These morphology properties qualitatively correlate with previous simulations and measurements [31, 36, 52].

The floating structure of positive SDBD leads to a weaker charge deposition along the dielectric compared to that of negative streamers. Due to this essential difference in the discharge structure, significant discrepancies in discharge development appear between the two polarities.

The calculated spatial and temporal evolution of surface charges for both polarities are shown in figure 3. The data are displayed in logarithmic form to make the regions with low surface charge density more apparent. In the cases without pre-pulse (single mode) for both polarities, the distribution of surface charges clearly indicates the trajectory of streamers, from which the longest distance achieved and the propagation velocity of streamers can be obtained. In general, the polarity of surface charges is consistent with that of the voltage pulse. However, during the voltage falling edge, the polarity of surface charges near the HV electrode is reversed, due to the backward breakdown between the HV electrode and the plasma channel.

The distribution of surface charges at the end of HV pulse in the single mode is used as the input for the subsequent discharge. Figures 3(a2) and (a3) show the behavior of surface charges during the positive pulse, with a negative or positive pre-pulse, respectively. In bipolar mode, residual surface charges are not fully neutralized and their polarity remains negative in most areas (x < 14.5 mm) after the streamer passes. Once the streamer exceeds the region covered by residual surface charges, the dielectric is again positively charged. Although the opposite polarity pre-pulse is applied, the largest propagation length is shorter than that of the single pulse. In contrast, the streamer trajectory in the unipolar mode can no longer be obtained through the surface charge profile.

With negative polarity, if a positive pre-pulse is applied (bipolar mode), the polarity of residual charges changes immediately after the streamer passes and the largest discharge length is further extended compared to that of the single mode (figure 3(b2)). When the pre-pulse has the same polarity (unipolar mode), the residual positive surface charges are first

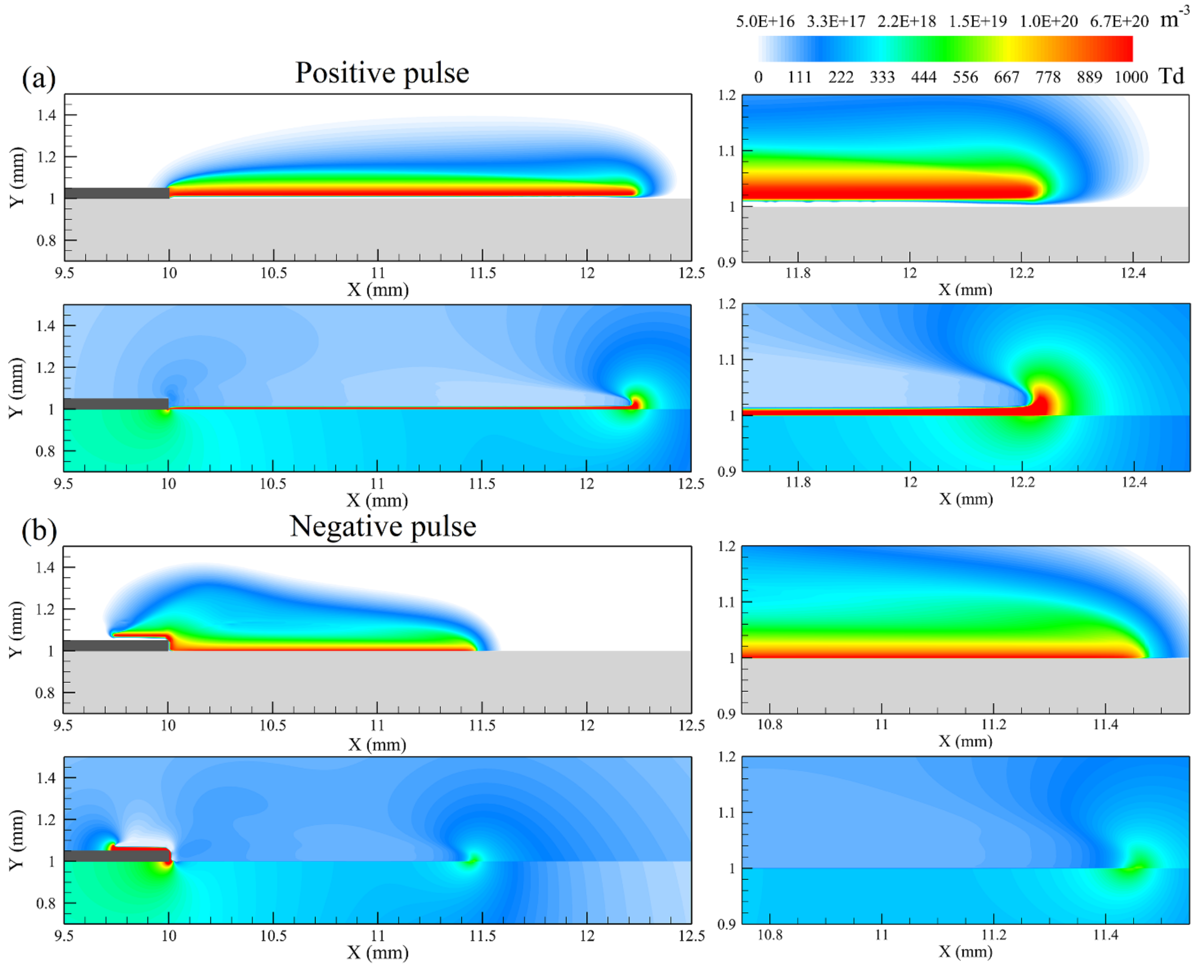

Figure 2. Distribution of electron density (unit in m^{-3}) and electric field (unit in Td) of SDBD with positive (a) and negative (b) polarity in single mode. Time instance is 6.5 ns for both cases. The regions near the streamer front are enlarged (right column).

erased around 6 ns, and then left again during the voltage falling edge (figure 3(b3)).

As shown in figure 3, when the discharge is operated in the bipolar mode, the polarity of deposited surface charges during the current pulse has the opposite sign with that of the residual charges, which significantly enhances the net transferred charges. The discharge operated in the bipolar mode has more transferred surface charges (line density of 0.296 μC m^{-1} for positive and 0.738 μC m^{-1} for negative polarity) than that in the unipolar mode (0.077 μC m^{-1} for positive and 0.094 μC m^{-1} for negative polarity), by a factor of 3–8. This verifies the experimental results in [52], that transfer surface charges in the alternating polarity mode are about a factor of 5 higher compared to those in the single polarity mode.

In order to illustrate the impact of residual surface charges on the dynamics of SDBD, the calculated discharge front location and the corresponding instantaneous velocity of both polarities are presented in figure 4. The position of the maximal electric field taken along a line 10 μm above the dielectric is selected to represent the location of the discharge front. Two typical features can be observed in all cases: (a) the breakdown occurs earlier if the discharge operates in the bipolar mode, while it is delayed in the unipolar mode; (b) the velocity first increases at the early stage of the propagation, reaches the maximum, and then descends verse time. The change in the discharge length and the streamer velocity is directly related to the deposition of surface charges.

With positive polarity, the largest discharge length is obtained in the single mode. Although the propagation trajectory and the velocity trend in the unipolar mode are similar to those in the single mode, the maximal velocity is reduced, for which the positive residual surface charges slightly suppress the discharge development. In the bipolar mode, the impact of residual charges on discharge development is complex. Near the HV electrode, an enhancement effect can be observed since the discharge ignites earlier. However, as the SDBD propagates close to the edge of the region covered by residual surface charges (∼4 mm from the HV electrode), the velocity drops dramatically, showing a strong suppression effect. This is due to the fact that the negative SDBD in pre-pulse propagates a shorter length than that of the positive polarity, and the deposition of residual surface charges decreases along the dielectric (non-uniform distribution). Out of this area, the velocity first rises again and then descends with decreasing voltage.

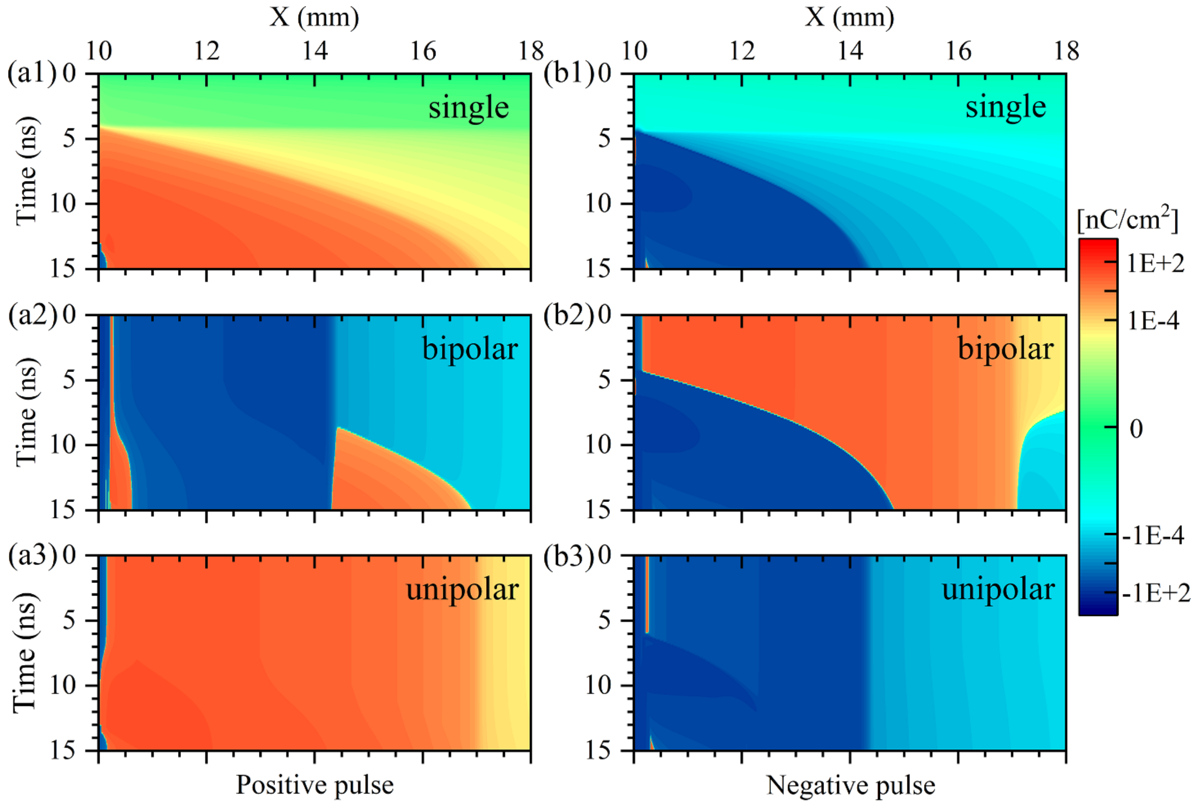

Figure 3. Spatial and temporal evolution of the surface charge density in single ((a1) and (b1)), bipolar ((a2) and (b2)), and unipolar ((a3) and (b3)) modes. The left column is for positive polarity, and the right for negative.

With negative polarity, the bipolar mode has the largest discharge length and maximal instantaneous velocity. The pre-pulse with opposite polarity greatly enhances the development of the negative streamer. In the unipolar mode, although the instantaneous velocity is comparable to the other two modes, a shorter discharge length is obtained due to faster drop rate in the velocity.

Dynamics of SDBD plasma are monitored by an intensified charge-coupled device (ICCD camera) in [52], which indicates that the velocity of negative surface discharge is lower than that during the positive polarity pulse with a similar peak voltage. Similarly, from figure 4, a common feature can also be observed that the maximum velocity of the negative streamer is lower than that of the positive polarity and the velocity of the negative streamer drops more rapidly after its peak.

3.2. Energy deposition

Figures 5(a) and (b) present the spatial distribution of the energy density. Several features in common for both polarities can be found: (a) the largest energy density appears near the HV electrode, and the value decreases with increasing distance along the dielectric; (b) when the discharge operates in the bipolar mode, the spatial range in the y direction is extended; otherwise, the range shrinks.

Despite the similarities, the difference between positive and negative polarities caused by the pre-pulse is obvious. For the negative pulse, the coverage of the energy density in the x direction sharply reduces in the unipolar mode, while it obviously expands forward in the bipolar mode. However, for the positive pulse, the energy density range shrinks in the x direction regardless of the pre-pulse polarity.

Figure 5(c) shows the distribution of the energy density taken along a line 10 μm above the dielectric. For the positive pulse, the profiles of the energy density between the single and unipolar modes are very close. In contrast, the energy density in the bipolar mode is much weaker, in the range of 10–11 mm, but rises to a higher value in the range of 11–14 mm. It is worth noting that the polarities of the surface charges deposited in these two regions are exactly opposite, as shown in figure 3(a2).

As for the negative pulse, the impact of the pre-pulse or residual surface charges is very much clear. In the bipolar mode, most areas of the dielectric are positively charged at the inception moment except near the HV electrode, significantly enhancing energy deposition. On the contrary, the energy density in the unipolar mode is lower along the discharge channel with the presence of the negative residual surface charges.

By calculating the product of the energy density and the volume of each cell and summing it over the plasma domain, the total energy can be obtained. From figure 5(d), it can be seen that, for both polarities, the total energy is significantly enhanced in the bipolar mode while it is weakened in the unipolar mode. A higher coupled energy during the discharge pulse is accompanied by more transferred surface charges, which is consistent with the experimental observations [52].

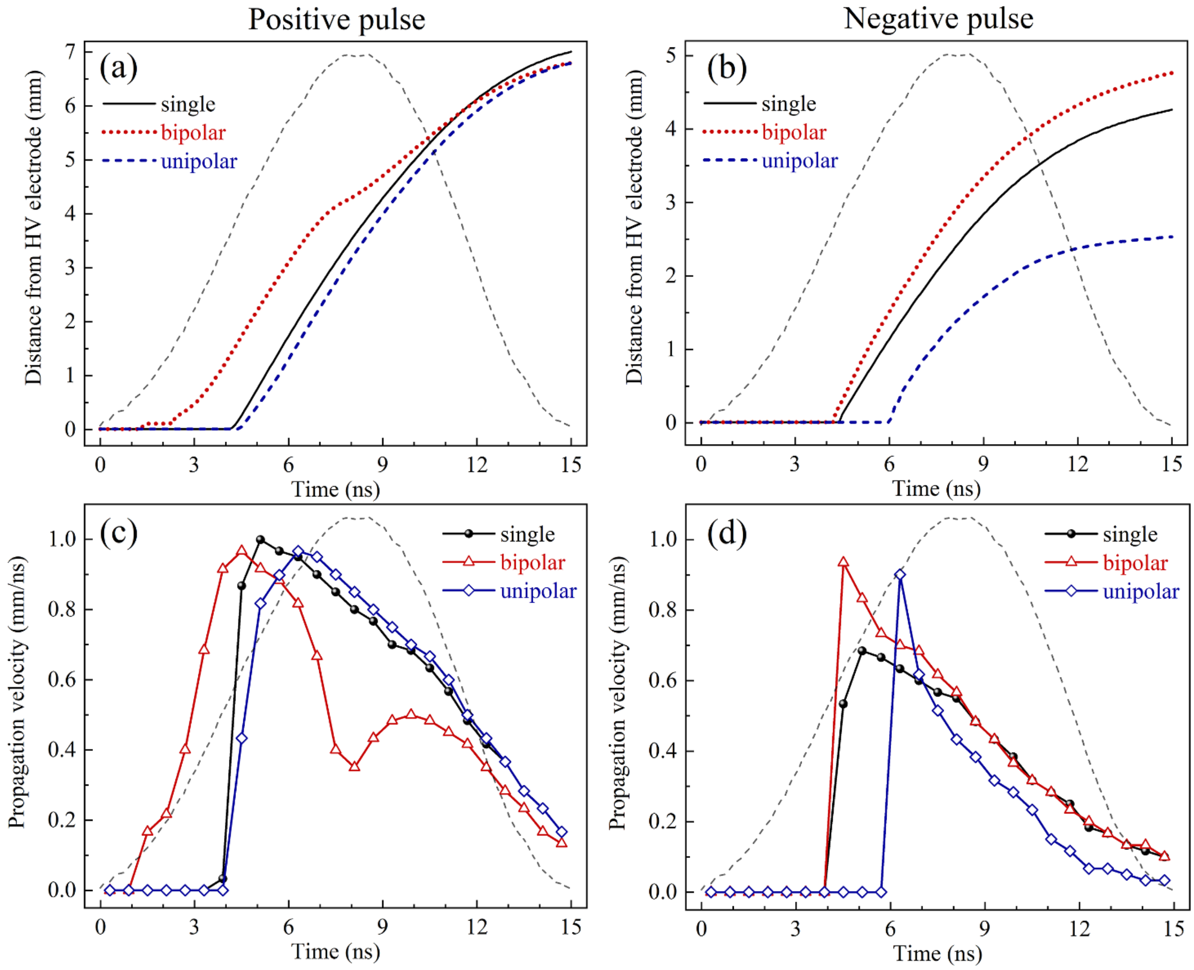

Figure 4. Dynamics (location and velocity) of SDBD propagation operated in single, bipolar, and unipolar modes. The left column is for positive polarity ((a) and (c)), and the right for negative ((b) and (d)).

3.3. Evolution of electric field

Electric field vector components in SDBDs have been measured by picosecond E-FISH for positive, negative, and alternating polarity pulse trains [23]. The results demonstrate a significant electric field offset before the discharge pulse and directly confirm that the charge accumulation along the dielectric plays an important role in SDBDs.

Here, figures 6 and 7 present the calculated temporal evolutions of the horizontal and vertical electric field components (E_x and E_y) for both polarities operated in the single, bipolar, and unipolar modes, respectively. The field components are taken at different locations in the x direction, and 5 μm above the dielectric in the y direction. The position 200 μm away from the HV electrode is referred to as HV in these two figures. E_x and E_y are positive when pointing away from the HV electrode or the dielectric surface, respectively.

The results of positive polarity are plotted in figure 6. Note that the axis of E_y is inverted to make the comparison more apparent. In the single mode, both E_x and E_y increase from zero as the voltage starts to rise, as shown in figure 6(a). After reaching the peak value, both components near the HV electrode first drop considerably, indicating the breakdown occurs, and then increase again as the voltage continues to rise. Subsequently, the fields at locations further away from the HV electrode sequentially reach the peak and diminish with the decrease in voltage, corresponding to the forward propagation of the streamer. On the voltage falling edge, E_x near the HV electrode reverses and reaches its negative peak, indicating that a reverse breakdown occurs.

In the bipolar mode, from figure 6(b), both E_x and E_y are of non-zero value at the beginning of the voltage pulse due to the residual surface charges accumulated in the previous pulse. At this instant, the direction of E_x is determined by the difference in the deposited charge density between the local and adjacent regions, while the direction of E_y largely depends on the polarity of the local surface charges. Thus, within the residual charge area (figure 3(a2)), E_x points to the HV electrode, while E_y points to the dielectric. Due to the presence of residual surface charges, the discharge starts earlier and the breakdown voltage drops significantly. After the voltage starts to rise, E_x decreases to zero and increases again in the opposite direction (now pointing away from the HV electrode). At the end of the voltage pulse, E_x presents an obvious negative offset while E_y

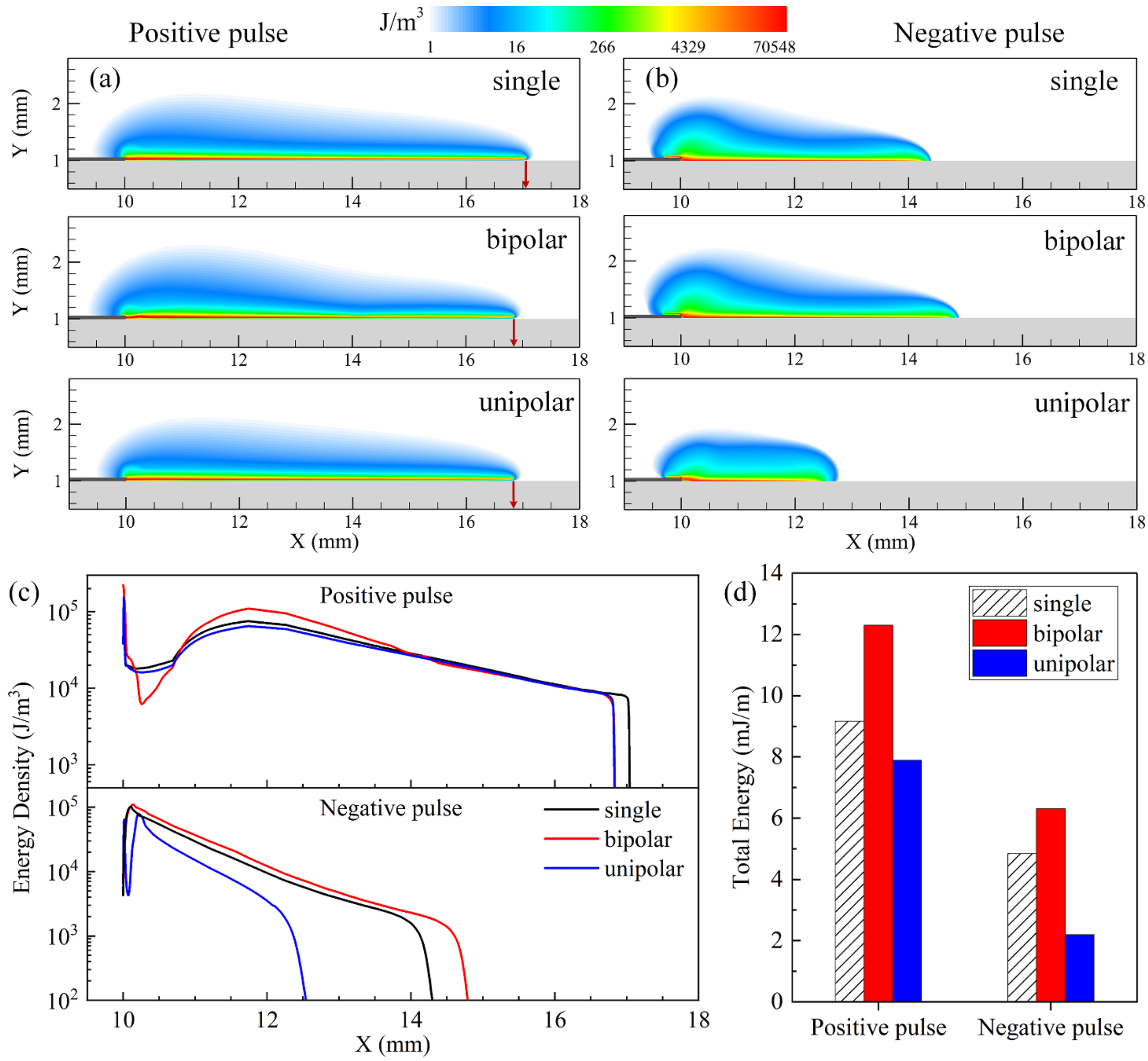

Figure 5. Spatial distribution of the energy density in single, bipolar, and unipolar modes for positive (a) and negative (b) polarity. Comparison of energy density along the line 10 μm above the dielectric (c) and the total energy deposited over the plasma domain (d).

approaches almost zero. Similar results are also observed in experiments [23].

In the unipolar mode (figure 6(c)), it can be seen that E_x near the HV electrode is clearly a non-zero value before the voltage pulse. The negative E_x is generated by the residual negative charges during the reverse breakdown of the previous pulse (figure 3(a3)). At locations far away from the HV electrode, weak positive charges are deposited in the pre-pulse, and thus no significant residual fields appear. Both E_x and E_y at HV present a two-peak feature. Compared to the bipolar mode, a steeper profile for both field components is obtained at the breakdown instance. Except for a slight delay in the breakdown instance, the subsequent evolutions are similar to those of the single mode.

Figure 7 presents the temporal evolutions of electric field components for negative polarity. The axes of E_x and voltage are inverted. It is observed in figure 6 that for the positive pulse, the absolute value of the E_y component is much higher than the E_x component, which is not the case for the negative pulse (figure 7). The reason of these differences lies in that the thin ion-rich layer with local enhanced electric field is found with the positive SDBD, while the negative SDBD keeps a diffuse shape and no gap is formed between the discharge channel and the dielectric. Thus, E_y in the negative SDBD has a much weaker amplitude compared to that of the positive one.

From figure 7(b), at the inception of the voltage pulse, a negative E_x and a positive E_y can be observed near the HV electrode. The directions of field components are consistent with those of the applied voltage. Thus, with increasing voltage, the discharge is enhanced by the residual charges, and the breakdown occurs at an earlier instance. E_x also presents a two-peak feature, but, the second peak has a lower amplitude compared to the first one, and no longer exhibits a near-Laplacian behavior. After the discharge front passes by, E_y drops much rapidly to almost zero compared to that of positive, showing a strong self-shielding effect at the same vertical distance above the dielectric. On the voltage falling edge, E_y near the HV electrode is dominated by the local surface charge density and

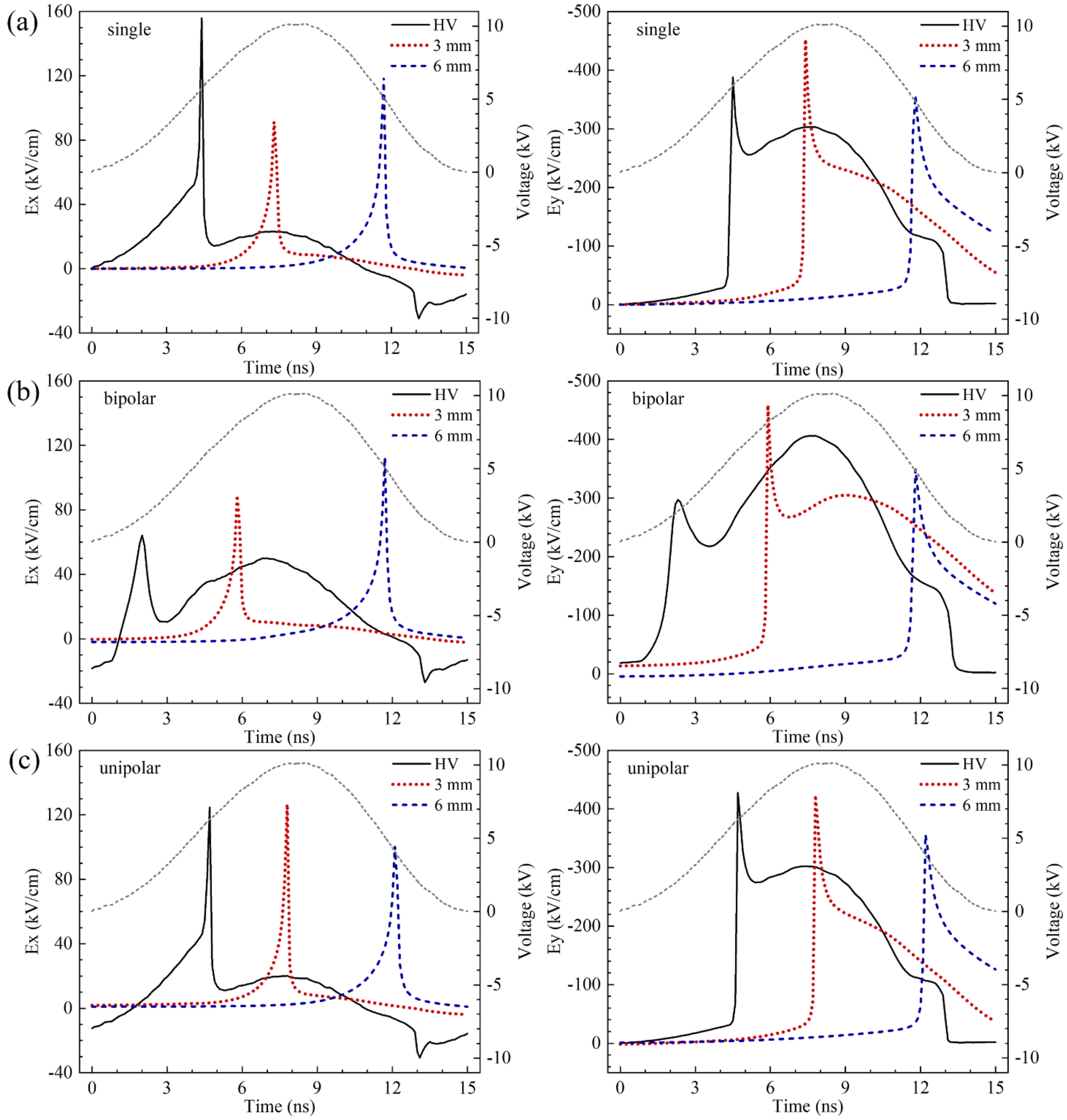

Figure 6. Temporal evolution of the electric field vector components at different locations from the HV electrode for positive pulse operated in single (a), bipolar (b), and unipolar (c) modes. The left column is for the horizontal components E_x and the right for the vertical components E_y.

increases in the reverse direction (pointing to the dielectric surface), which will further enhance the subsequent positive discharge.

From figure 7(c), in the unipolar mode, both E_x and E_y show a Laplacian profile and no abrupt reduction appears near the HV electrode. During the voltage falling edge, E_x first shows a negative offset and then decreases as the voltage approaches zero. With increasing distance from the HV electrode, the negative offset in E_x reduces. This behavior qualitatively correlates with the findings in [23]. E_y first decreases to zero and then increases in the opposite direction to facilitate the discharge. The breakdown voltage is much higher, and the field components have a peak lower than that of the single mode. With the decrease of voltage, E_y rises significantly in the negative direction and reaches its maximum around -180 kV cm^{-1} at the end of the voltage pulse. This is attributed to the strong accumulation of negative surface charges. Thus, in the next pulse, electrons will be pushed away from the HV electrode and the discharge will be further suppressed.

The most distinct difference between the measurement and simulation is that the amplitude of the measured electric field is about 10–20 kV cm^{-1} [23], while the calculated value is almost an order of magnitude higher. Such a high electric field has also been reported in previous simulations [34, 36, 58]. At a position close to the dielectric surface, the electric field is mainly determined by the local net space/surface charge.

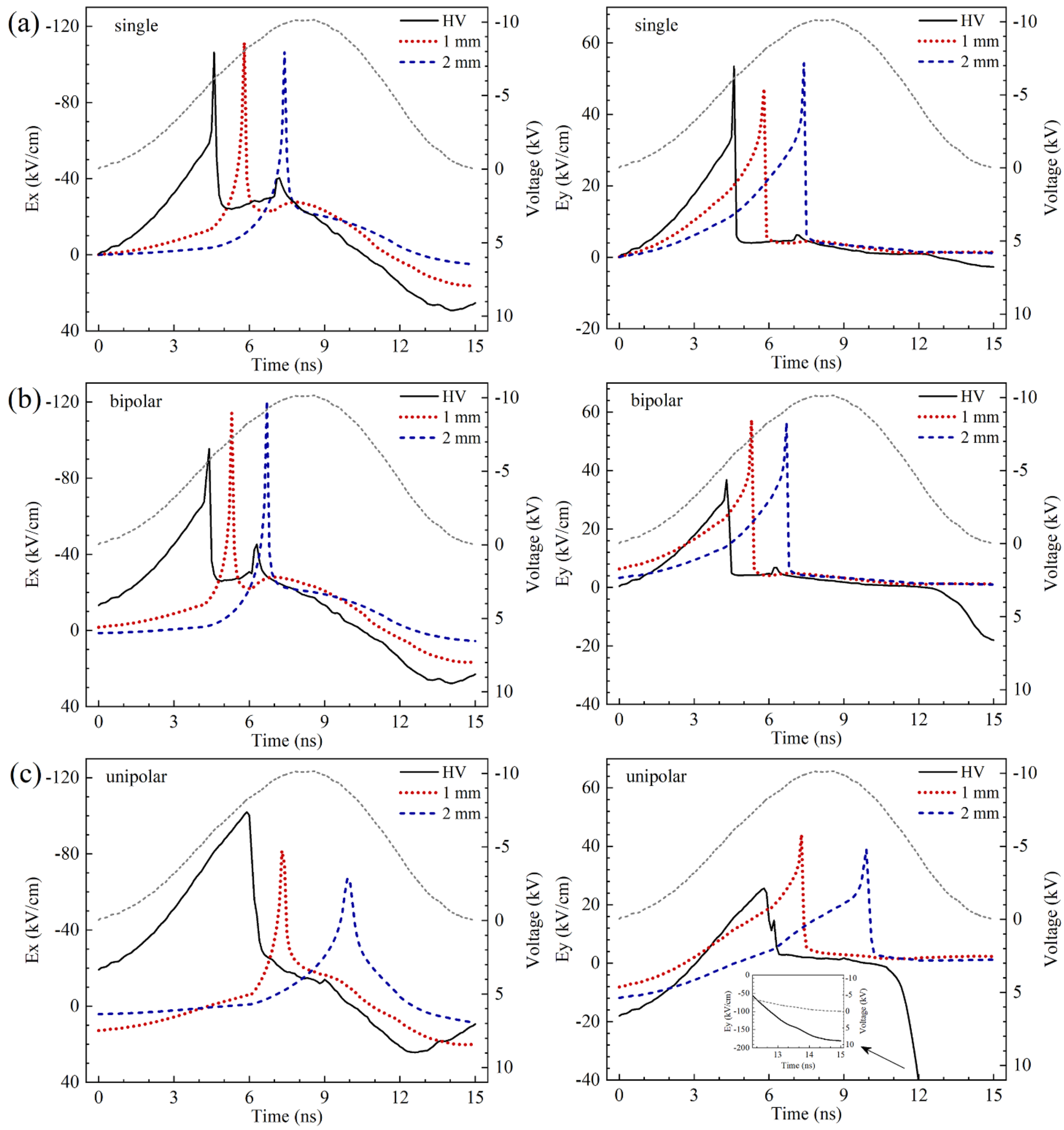

Figure 7. Temporal evolution of the electric field vector components at different locations from the HV electrode for negative pulse operated in single (a), bipolar (b), and unipolar (c) modes. The left column is for the horizontal components E_x and the right for the vertical components E_y.

With increasing distance from the surface, the electric field is a superposition of the Laplacian field created by applied voltage and the field from the net space/surface charge. As a result, the electric field (shown in figure 2) quickly decreases with the increase of the height above the surface [36].

The picosecond E-FISH in [23] has a very high temporal resolution to capture the evolution of surface discharge. However, the laser beam diameter near the focal point is $\sim$200 μm. This indicates that the laser beam may be positioned above the near-surface plasma or the electric field is measured in the nearly completely self-shielded plasma [23].

3.4. Limitations

In fact, as the streamer-to-filament transition in surface discharge occurs, the 2D fluid model is no longer suitable to describe this essentially 3D phenomenon. Also, under a high repetition rate, the role of fast gas heating in the discharge channel and the memory effect of residual space charges needs to be incorporated [59, 60]. These are beyond the scope of the model used in this work. For further investigation, several improvements could be performed, including a detailed kinetics scheme of excited species for fast gas heating, a fully kinetic treatment of electrons, an introduction of stochastic processes, or a 3D model for interactions between surface streamers.

4. Conclusions

In this work, the structure, dynamics, and energy deposition of positive and negative SDBDs are numerically analyzed by a 2D fluid model, with the consideration of residual charges on the dielectric. By preserving the distribution of surface charges at the end of the previous HV pulse, the impact of residual surface charges on the subsequent discharge is introduced. Based on this assumption, discharges operated in the single, bipolar, and unipolar modes for both polarities are presented.

An essential difference between the positive and negative SDBDs is observed. With positive polarity, SDBD is floating above the dielectric, forming an ion-rich region with an intense electric field near the surface. The negative SDBD directly contacts the dielectric and charges it. Consequently, the properties of surface charge deposition differ greatly between the two polarities. It is worth noting that the reversal of surface charge polarity near the HV electrode can be observed during the voltage falling edge for both positive and negative SDBDs.

The energy deposition and dynamics of surface discharges in the three modes are compared. The total energy deposited in the gas phase is significantly enhanced in the bipolar mode, while it is suppressed in the unipolar mode. From the temporal evolutions of electric field components, the well-pronounced forward propagation processes are obtained. With the accumulation of surface charges in the previous pulse, both electric field components are non-zero at the inception of the current discharge. In the bipolar mode, the field directions induced by residual surface charges coincide with those of the applied voltage, which greatly reduces the breakdown voltage and enables the discharge to start earlier. In the unipolar, the opposite effects are observed.

The present work demonstrates the critical importance of residual surface charges on the repetitively pulsed SDBDs, providing a reference for the regulation of their breakdown process and energy deposition.

Data availability statement

All data that support the findings of this study are included within the article (and any supplementary files)

Acknowledgments

This work was supported by National Key R&D Program of China (Grant No. 2021YFB2401400), the National Science Fund for Distinguished Young Scholars (Grant No. 51925703), the National Natural Science Foundation of China (Grant Nos. 52022096, 51907190), the Young Elite Scientist Sponsorship Program by CAST (Grant No. YESS20210402), and the State Key Laboratory of Alternate Electrical Power System with Renewable Energy Sources (Grant No. LAPS22018). The authors are thankful to Dr Yifei Zhu for fruitful discussions.

ORCID iDs

Chenhua Ren https://orcid.org/0000-0002-7163-1171
Bangdou Huang https://orcid.org/0000-0002-1523-7380
Cheng Zhang https://orcid.org/0000-0003-1512-2820
Bo Qi https://orcid.org/0000-0001-8001-5824
Tao Shao https://orcid.org/0000-0002-5738-1241

References

[1] Popov N A and Starikovskaia S M 2022 Relaxation of electronic excitation in nitrogen/oxygen and fuel/air mixtures: fast gas heating in plasma-assisted ignition and flame stabilization *Prog. Energy Combust. Sci.* **91** 100928
[2] Starikovskaia S M 2014 Plasma-assisted ignition and combustion: nanosecond discharges and development of kinetic mechanisms *J. Phys. D: Appl. Phys.* **47** 353001
[3] Brandenburg R 2017 Dielectric barrier discharges: progress on plasma sources and on the understanding of regimes and single filaments *Plasma Sources Sci. Technol.* **26** 053001
[4] Eto H, Ono Y, Ogino A and Nagatsu M 2008 Low-temperature sterilization of wrapped materials using flexible sheet-type dielectric barrier discharge *Appl. Phys. Lett.* **93** 221502
[5] Zhang C, Huang B D, Luo Z B, Che X K, Yan P and Shao T 2019 Atmospheric-pressure pulsed plasma actuators for flow control: shock wave and vortex characteristics *Plasma Sources Sci. Technol.* **28** 064001
[6] Leonov S B, Adamovich I V and Soloviev V R 2016 Dynamics of near-surface electric discharges and mechanisms of their interaction with the airflow *Plasma Sources Sci. Technol.* **25** 063001
[7] Deng J B, Matsuoka S, Kumada A and Hidaka K 2010 The influence of residual charge on surface discharge propagation *J. Phys. D: Appl. Phys.* **43** 495203
[8] Li C Y, Lin C J, Chen G, Tu Y P, Zhou Y, Li Q, Zhang B and He J L 2019 Field-dependent charging phenomenon of HVDC spacers based on dominant charge behaviors *Appl. Phys. Lett.* **114** 202904
[9] Florkowski M, Krzesniak D, Kuniewski M and Zydron P 2020 Surface discharge imaging in presence of deposited space charges in non-uniform DC electric field *High Volt.* **6** 576–89
[10] Yu S Q, Yan H J, Li J Q, Li T, Wang Y Y and Song J 2022 Distribution and evolution of surface charge in surface dielectric barrier discharge driven by AC and pulse dual power supply *J. Appl. Phys.* **55** 125201
[11] Zhu Y F and Starikovskaia S 2018 Fast gas heating of nanosecond pulsed surface dielectric barrier discharge: spatial distribution and fractional contribution from kinetics *Plasma Sources Sci. Technol.* **27** 124007
[12] Huang B D, Zhang C, Adamovich I, Akishev Y and Shao T 2020 Surface ionization wave propagation in the nanosecond pulsed surface dielectric barrier discharge: the influence of dielectric material and pulse repetition rate *Plasma Sources Sci. Technol.* **29** 044001
[13] Kruszelnicki J, Ma R C and Kushner M J 2021 Propagation of atmospheric pressure plasmas through interconnected pores in dielectric materials *J. Appl. Phys.* **129** 143302
[14] Zhang Q Z, Zhang L, Yang D Z, Schulze J, Wang Y N and Bogaerts A 2020 Positive and negative streamer propagation in volume dielectric barrier discharges with planar and porous electrodes *Plasma Process. Polym.* **18** e2000234

[15] Jansky J, Bessieres D, Brandenburg R, Paillol J and Hoder T 2021 Electric field development in positive and negative streamers on dielectric surface *Plasma Sources Sci. Technol.* **30** 105008
[16] Kourtzanidis K, Dufour G and Rogier F 2021 Self-consistent modeling of a surface AC dielectric barrier discharge actuator: in-depth analysis of positive and negative phases *J. Appl. Phys.* **54** 045203
[17] Sato S, Mitsuhashi K, Enokido T, Komuro A, Ando A and Ohnishi N 2021 Surface-charge control strategy for enhanced electrohydrodynamic force in dielectric barrier discharge plasma actuators *J. Appl. Phys.* **54** 455203
[18] Zhang B Y and Zhang G X 2017 Interpretation of the surface charge decay kinetics on insulators with different neutralization mechanisms *J. Appl. Phys.* **121** 105105
[19] Zhao Z and Li J T 2020 Repetitively pulsed gas discharges: memory effect and discharge mode transition *High Volt.* **5** 569–82
[20] Zhao Z, Huang D D, Wang Y N, Li C J and Li J T 2020 Volume and surface memory effects on evolution of streamer dynamics along gas/solid interface in high-pressure nitrogen under long-term repetitive nanosecond pulses *Plasma Sources Sci. Technol.* **29** 015016
[21] Takashima K, Zuzeek Y, Lempert W R and Adamovich I V 2011 Characterization of a surface dielectric barrier discharge plasma sustained by repetitive nanosecond pulses *Plasma Sources Sci. Technol.* **20** 055009
[22] Sokolova M V, Voevodin V V, Malakhov J I, Aleksandrov N L, Anokhin E M and Soloviev V R 2019 Barrier properties influence on the surface dielectric barrier discharge driven by single voltage pulses of different duration *J. Phys. D: Appl. Phys.* **52** 324001
[23] Simeni Simeni M, Tang Y, Frederickson K and Adamovich I V 2018 Electric field distribution in a surface plasma flow actuator powered by ns discharge pulse trains *Plasma Sources Sci. Technol.* **27** 104001
[24] Huang B D, Zhang C, Zhu W C, Lu X P and Shao T 2021 Ionization waves in nanosecond pulsed atmospheric pressure plasma jets in argon *High Volt.* **6** 655–73
[25] Stollenwerk L, Laven J G and Purwins H G 2007 Spatially resolved surface-charge measurement in a planar dielectric-barrier discharge system *Phys. Rev. Lett.* **98** 255001
[26] Mitsuhashi K, Komuro A, Suzuki K, Natsume C and Ando A 2021 Spatiotemporal variations of the electrical potential on surface dielectric barrier discharges *Plasma Sources Sci. Technol.* **30** 04LT02
[27] Li T, Yan H J, Li J Q, Schulze J, Yu S Q, Song J and Zhang Q Z 2022 The role of surface charge and its decay in surface dielectric barrier discharges *Plasma Sources Sci. Technol.* **31** 055016
[28] Zhang Q Z, Nguyen-Smith R T, Beckfeld F, Liu Y, Mussenbrock T, Awakowicz P and Schulze J 2021 Computational study of simultaneous positive and negative streamer propagation in a twin surface dielectric barrier discharge via 2D PIC simulations *Plasma Sources Sci. Technol.* **30** 075017
[29] Zhao P, Gu J G, Wang H Y, Zhang Y, Xu X Y and Jiang W 2020 How bead shapes affect the plasma streamer characteristics in packed-bed dielectric barrier discharges: a kinetic modeling study *Plasma Sci. Technol.* **22** 034013
[30] Unfer T and Boeuf J P 2009 Modelling of a nanosecond surface discharge actuator *J. Phys. D: Appl. Phys.* **42** 194017
[31] Stepanyan S A, Soloviev V R and Starikovskaia S M 2014 An electric field in nanosecond surface dielectric barrier discharge at different polarities of the high voltage pulse: spectroscopy measurements and numerical modeling *J. Phys. D: Appl. Phys.* **47** 485201
[32] Viegas P, Slikboer E, Obrusnik A, Bonaventura Z, Sobota A, Garcia-Caurel E, Guaitella O and Bourdon A 2018 Investigation of a plasma-target interaction through electric field characterization examining surface and volume charge contributions: modeling and experiment *Plasma Sources Sci. Technol.* **27** 094002
[33] Li X R, Sun A B, Zhang G J and Teunissen J 2020 A computational study of positive streamers interacting with dielectrics *Plasma Sources Sci. Technol.* **29** 065004
[34] Konina K, Kruszelnicki J, Meyer M E and Kushner M J 2022 Surface ionization waves propagating over non-planar substrates: wavy surfaces, cut-pores and droplets *Plasma Sources Sci. Technol.* **31** 115001
[35] Babaeva N Y 2015 Hot secondary electrons in dielectric barrier discharges treated with Monte Carlo simulation: implication for fluxes to surfaces *Plasma Sources Sci. Technol.* **24** 034012
[36] Babaeva N Y, Tereshonok D V and Naidis G V 2016 Fluid and hybrid modeling of nanosecond surface discharges: effect of polarity and secondary electrons *Plasma Sources Sci. Technol.* **25** 044008
[37] Pechereau F, Bonaventura Z and Bourdon A 2016 Influence of surface emission processes on a fast-pulsed dielectric barrier discharge in air at atmospheric pressure *Plasma Sources Sci. Technol.* **25** 044004
[38] Moreau E, Bayoda K and Benard N 2021 Streamer propagation and pressure waves produced by a nanosecond pulsed surface sliding discharge: effect of the high-voltage electrode shape *J. Appl. Phys.* **54** 075207
[39] Ding C, Jean A, Popov N A and Starikovskaia S M 2022 Fine structure of streamer-to-filament transition in high-pressure nanosecond surface dielectric barrier discharge *Plasma Sources Sci. Technol.* **31** 045013
[40] Opaits D F, Shneider M N, Miles R B, Likhanskii A V and Macheret S O 2008 Surface charge in dielectric barrier discharge plasma actuators *Phys. Plasmas* **15** 073505
[41] Boeuf J P, Lagmich Y and Pitchford L C 2009 Contribution of positive and negative ions to the electrohydrodynamic force in a dielectric barrier discharge plasma actuator operating in air *J. Appl. Phys.* **106** 023115
[42] Unfer T and Boeuf J P 2010 Modeling and comparison of sinusoidal and nanosecond pulsed surface dielectric barrier discharges for flow control *Plasma Phys. Control. Fusion* **52** 124019
[43] Zhu Y F, Chen X C, Wu Y and Starikovskaia S M 2021 PASSKEy code[software] (Paris: Science and Technology of Plasma Dynamics Laboratory, Xi'an, China and Laboratoire de Physique des Plasmas) (available at: www.plasma-tech.net/parser/passkey/)
[44] Zhu Y F, Shcherbanev S, Baron B and Starikovskaia S 2017 Nanosecond surface dielectric barrier discharge in atmospheric pressure air: i. measurements and 2D modeling of morphology, propagation and hydrodynamic perturbations *Plasma Sources Sci. Technol.* **26** 125004
[45] Hagelaar G J M and Pitchford L C 2005 Solving the Boltzmann equation to obtain electron transport coefficients and rate coefficients for fluid models *Plasma Sources Sci. Technol.* **14** 722–33
[46] Naidis G V 2006 On photoionization produced by discharges in air *Plasma Sources Sci. Technol.* **15** 253–5
[47] Bourdon A, Pasko V P, Liu N Y, Celestin S, Segur P and Marode E 2007 Efficient models for photoionization produced by non-thermal gas discharges in air based on radiative transfer and the Helmholtz equations *Plasma Sources Sci. Technol.* **16** 656–78
[48] Ren C H, Huang B D, Qiu J T, Zhang C, Qi B, Chen W J and Shao T 2022 Is an extended barrier-free discharge under nanosecond-pulse excitation really diffuse? *J. Appl. Phys.* **55** 235204

[49] Li S K, Huang B D, Zhang C and Shao T 2021 Development and application of all-solid-state bi-polar nanosecond pulse generators *High Power Laser Part. Beams* **33** 065005
[50] Babaeva N Y and Naidis G V 2016 Modeling of streamer dynamics in atmospheric-pressure air: influence of rise time of applied voltage pulse on streamer parameters *IEEE Trans. Plasma Sci.* **44** 899–902
[51] Naidis G V, Tarasenko V F, Babaeva N Y and Lomaev M I 2018 Subnanosecond breakdown in high pressure gases *Plasma Sources Sci. Technol.* **27** 013001
[52] Leonov S B, Petrishchev V and Adamovich I V 2014 Dynamics of energy coupling and thermalization in barrier discharges over dielectric and weakly conducting surfaces on μs to ms time scales *J. Phys. D: Appl. Phys.* **47** 465201
[53] Zhu Y F and Wu Y 2020 The secondary ionization wave and characteristic map of surface discharge plasma in a wide time scale *New J. Phys.* **22** 103060
[54] Pancheshnyi S, Nudnova M and Starikovskii A 2005 Development of a cathode-directed streamer discharge in air at different pressures: experiment and comparison with direct numerical simulation *Phys. Rev.* E **71** 016407
[55] Pancheshnyi S and Starikovskii A 2004 Stagnation dynamics of a cathode-directed streamer discharge in air *Plasma Sources Sci. Technol.* **13** B1–5
[56] Raizer Y P 1991 *Gas Discharge Physics* (Berlin: Springer)
[57] Soloviev V R and Krivtsov V M 2009 Surface barrier discharge modelling for aerodynamic applications *J. Phys. D: Appl. Phys.* **42** 125208
[58] Soloviev V R and Krivtsov V M 2018 Numerical modelling of nanosecond surface dielectric barrier discharge evolution in atmospheric air *Plasma Sources Sci. Technol.* **27** 114001
[59] Popov N A 2011 Fast gas heating in a nitrogen-oxygen discharge plasma: i. Kinetics mechanism *J. Phys. D: Appl. Phys.* **44** 285201
[60] Huang B D, Zhang C, Sun H, Sorokin D A, Tarasenko V F and Shao T 2022 Enhancement of hydrogen radical density in atmospheric pressure plasma jet by a burst of nanosecond pulses at 1MHz *Plasma Sources Sci. Technol.* **31** 025019